Design of a Single-Phase Common Mode and Differential Mode Inductor for Interleaved Converters

Jonathan Robinson, Gopal Mondal, Stefan Hänsel, Matthias Neumeister
SIEMENS AG
Erlangen, Germany
E-Mail: robinson.jonathan@siemens.com; gopal.mondal@siemens.com;
stefan.haensel@siemens.com, matthias.neumeister@siemens.com

Abstract

This paper analyses the design of single-phase interleaved inductors to provide inductance for differential mode (DM) circulating currents and common mode (CM) grid currents. The main design equations and a design optimization method are given. Comparison with other filter methods for equivalent performance shows reduced size with equivalent losses. Additional benefits using mixed core materials or due to phase shift in flux density are analyzed. Initial test results of a 120 kW converter demonstrate operation of the concept with a custom assembly that integrates the power electronics and coupled inductors in a combined heatsink.

1 Introduction

Interleaved converters for grid operation offer interesting potential to reduce the filter size while maintaining the same converter switching frequency and overall device losses. While in theory the concept can be used with any grid converter the real benefits from it are in applications requiring light weight converters in confined areas, such as mobility and offshore environments, especially at higher powers where parallel power modules would be normally required.

The main concept is shown in Fig. 1, where three interleaved converter modules are interconnected through the coupled DM inductor (L_{dmi}) and then connected to the grid through a 3-phase inductor (L_{cmi}).

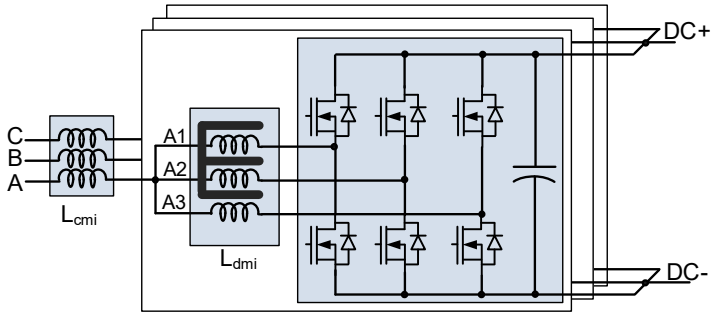

Fig. 1. Interleaved converter with coupled inductors to limit circulating current.

The dual-inductors have different purposes:

(a) L_{dmi}—this inductor limits circulating current between the parallel phases . By coupling the windings then only DM current (switching frequency circulating currents) will generate flux in the core. It is important that this inductor is connected across the interleaved phases (i.e. A1, A2, A3) and not between the grid phases.

(b) L_{cmi}—this inductor sees no switching frequency components (they are controlled to completely cancel at the common point between the interleaved sections) but is required for 50 Hz voltage regulation and filtering of higher order components (nf_{sw} where n is a multiple of the number of interleaved sections.

Note that CM and DM have been defined in the context of the coupled inductors and are different than the usual use of the terms. CM currents correspond to the main grid current (50 Hz) as well as harmonics

of the order $n_{int}f_{sw}$. DM currents are generated from the out-of-phase switching, with the main harmonic at the switching frequency. These harmonics cancel at the grid side of the coupled inductor where the terminals are connected.

It is also possible to include additional capacitors and inductors to create higher order filters. The design of L_{cmi} and any additional filter components have an important advantage, that the harmonics they see are at a much higher frequency than the switching frequency of the converter. When the interleaved inductors see low frequency fundamental flux and high frequency circulating currents, then the core must be optimized for both, which is a difficult engineering task. Using coupled inductors, as shown in Fig. 1, splits the design into two parts—a high-frequency inductor design (L_{dmi}) and a low frequency inductor design (L_{cmi}).

However, it has been noted that peak flux densities of the interleaved section may be out of phase with the grid currents [1], and therefore it is possible to allow some additional fundamental flux to flow in the coupled inductors to maximize the utilization of the inductor. Example extensions to this concept have been proposed in [2], [3]. In [2] both a single-phase and a 3-phase inductor design were proposed and advantages of both were derived, however no detailed information was given on the design of the inductor nor a precise analyses on the benefits over a split inductor design. The design in [3] is similar to the single-phase design, although with only an additional core for common-mode flux and no additional winding (note that in [3], only a two-winding inductor is described, but the concept can be extended for additional interleaved sections). A basic electrical and magnetic circuit diagram of both concepts for an application with three interleaved sections is shown in Fig. 2.

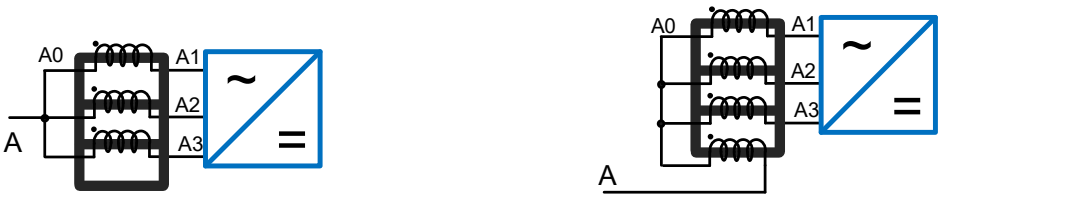

(a) Coupled inductor with common mode limb

(b) Coupled inductor with wound common mode limb

Fig. 2. Basic diagram of different CM/DM interleaved coupled inductors.

The additional winding gives an additional degree of engineering freedom (i.e. both air gap as well as the number of turns) for designing the inductor, but it is not clear what exactly the additional benefits of having this extra winding are in practice, nor is it clear if there are benefits over a split inductor design, which has the advantage that both inductors can be designed for either high-frequency or low-frequency flux. This paper studies the design of the single phase integrated CM and DM inductor to fully understand the design trade-offs and benefits of the concept. To simplify the analysis, only three interleaved sections will be considered, but all equations are easily adaptable for a different number.

2 Inductor Design Equations

The single-phase differential and common mode inductors are shown in Fig. 3. The DM flux (Fig. 3a) flows only between the interleaved windings since it is directly out of phase in other interleaved windings and get cancelled in the top and bottom limbs of the core and cannot then flow in the CM winding branch (W_{cm}). CM flux (Fig. 3b) will flow equally in the same direction of windings A1, A2, and A3, will then add up to 3x in the upper and lower limbs, and flow down the CM branch where winding W_{cm} is wound.

(a) Differential mode flux

(b) Common Mode flux

Fig. 3. Single phase differential and common mode inductor showing the different types of flux in the cores.

The inductance (L_{dmi}) and maximum flux density ($B_{dmi,max}$) for the differential section (windings W_1-W_3) are given by the basic inductance formulas as:

$$B_{dmi,max} = \frac{\mu_0 I_{dmi,pk} n_{dmi}}{l_{g,dmi}} \tag{1}$$

$$L_{dmi} = \frac{n_{dmi}^2 \mu_0 A_c}{l_{g,dmi}} \tag{2}$$

where n_{dmi} is the number of turns of the differential windings, A_c is the area of the core, and $l_{g,dmi}$ is the air gap. For the CM sections, similar equations for the maximum CM flux density ($B_{cmi,max}$) and CM inductance (L_{cmi}) can be derived as:

$$B_{cmi,max} = \frac{\varphi_{cmi}}{A_c} = \frac{\left(n_{dmi}\frac{I_{cmi}}{3} + n_{cmi} I_{cmi}\right)}{\frac{l_{g,dmi}}{3\mu_0} + \frac{l_{g,cmi}}{\mu_0}} \tag{3}$$

$$V_{cmi} = n_{dmi} \cdot \frac{1}{3}\frac{d\varphi_{cmi}}{dt} + n_{cmi}\frac{d\varphi_{cmi}}{dt} = \frac{\left(\frac{n_{dmi}}{3} + n_{cmi}\right)^2 \mu_0 A_c}{\left(\frac{l_{g,dmi}}{3} + l_{g,cmi}\right)} \cdot \frac{dI_{cmi}}{dt} = L_{cmi} \cdot \frac{dI_{cmi}}{dt} \tag{4}$$

where φ_{cmi} is the flux due to CM voltage across the winding, I_{cmi} is the CM current, and n_{cmi} is the number of turns for the CM winding, and $l_{g,cmi}$ is the total air gap for the CM core section. One aspect of (3) and (4) is that they use a common core area. When the core areas for the differential and CM sections are different then the equations can be modified as:

$$B_{cmi,max} = \frac{\mu_0 I_{cmi,pk}\left(\frac{n_{dmi}}{3} + n_{cmi}\right)}{\frac{l_{g,dmi}}{3}\frac{A_{c,cmi}}{A_{c,dmi}} + l_{g,cmi}} \tag{5}$$

$$L_{cmi} = \frac{\left(\frac{n_{dmi}}{3} + n_{cmi}\right)^2 \mu_0}{\left(\frac{l_{g,dmi}}{3A_{c,dmi}} + \frac{l_{g,cmi}}{A_{c,cmi}}\right)} \tag{6}$$

Note that the maximum CM current is given by the peak current at maximum power, while the maximum DM current can be obtained as described in [1].

Since the maximum DM current occurs around the zero crossing of the AC voltage (when the duty cycle is between 1/3 and 2/3—as shown in [1]) then the core utilization can be optimized for applications that require only active power at full power so that:

$$B_{dmcore,max} = B_{dmi,max} + k_r \frac{B_{cmi,max}}{3}\frac{A_{c,cmi}}{A_{c,dmi}} \tag{7}$$

and k_r is a factor varying from 2/3 to 1.

3 Optimized Design Methodology

Similar to other magnetic components, the optimum design is a trade-off between material cost, losses, and meeting the physical constraints of the materials, such as maximum temperature. In order to compare the designs in a basic way, then an optimization problem will be set up based on the dimension information shown in Fig. 4.

The following assumptions are made:

(a) The DM core will be considered square with side length d_c.
(b) The CM core will be considered rectangular with side length $d_c \cdot d_{c2}$.

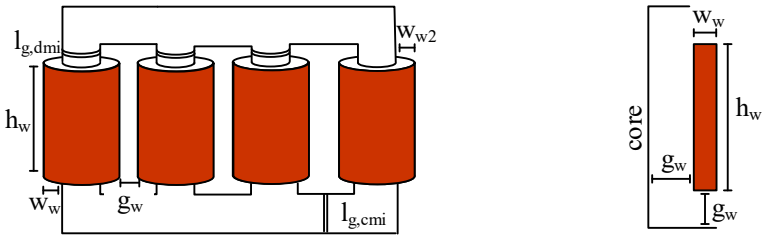

Fig. 4. Inductor dimensions for setting up optimization problem.

(c) The gaps between windings and between the windings and core (g_w) will be considered the same and equal to 2 mm.
(d) Dimensions of the winding (defined by w_w and h_w) will be increased by a factor k=1/0.75 to account for winding conductor insulation (this factor depends on the converter voltage).
(e) While the CM inductor is shown to the right of the interleaved inductors in Fig. 4, the ideal placement is in the middle, where the CM flux will then equally split in the different directions and reducing the required size of the upper and lower limbs. The design equations used here consider this ideal case.

The cost minimization function can then be defined as:

$$\underset{\underline{x}}{Min} = \{C_{cond} + C_{core} + C_{losses}\} \tag{8}$$

where the conductor cost (C_{cond}) depends on the cost of copper (C_{cu}) and conductor weight (M_{cu}):

$$C_{cond} = C_{cu} M_{cu} \tag{9}$$

the core cost (C_{core}) depends on the core material cost (C_{fe}) and core weight (M_{fe}):

$$C_{core} = C_{fe} M_{fe} \tag{10}$$

and cost of losses (C_{loss}) is calculated considering the present value of losses over N years, an interest rate i, and a cost per kWh of C_{kWh}:

$$C_{loss} = \frac{24 \cdot C_{kWh} E_{loss(kwh)}}{i}\left(1 - \frac{1}{(1+i)^N}\right) \tag{11}$$

It can be noted that C_u, C_{fe}, and C_{kWh} are effectively weighting functions that can be based on actual cost or modified to fulfill an objective (e.g. weight or loss minimization). The minimization variable $\underline{x}$, is defined as:

$$\underline{x} = \left[w_w \;\; l_w \;\; l_{g,dmi} \;\; d_c \;\; n_{dmi} \;\; J_{cond} \;\; B_{max,dmi} \;\; w_{w2} \;\; l_{g,dmi} \;\; n_{cmi} \;\; B_{max,cmi}\right] \tag{12}$$

where J_{cond} is the current density of the conductor and other variables are defined previously and in Fig. 4. The mass of the conductors is the total of the DM and CM conductor mass:

$$M_{cu,dmi} = 3 d_{cu} MLT_{dmi} n_{dmi} \frac{I_{rms,dmi}}{J_{cond}} \tag{13}$$

$$M_{cu,cmi} = d_{cu} MLT_{cmi} n_{cmi} \frac{I_{rms,cmi}}{J_{cond}} \tag{14}$$

where d_{cu} is the density of the conductor and MLT_{dmi} and MLT_{cmi} are the mean length per turn of the CM and DM windings, given by:

$$MLT_{dmi} = 4\left(d_c + 2g_w + \frac{w_w}{k}\right) \tag{15}$$

$$MLT_{cmi} = 4\left(\frac{d_c + d_{c2}}{2} + 2g_w + \frac{w_{w2}}{k}\right) \tag{16}$$

Similarly, the mass of the core can be calculated as the total of:

$$M_{fe,dmi} = d_{fe} d_c^2 \left(8\frac{w_w}{k} + 3\frac{h_w}{k} + 6d_c + 18g_w - 3l_{g,dmi} \right) \tag{17}$$

$$M_{fe,cmi} = d_{fe}(d_c \cdot d_{c2}) \left(2\frac{w_w}{k} + 2\frac{w_{w2}}{k} + \frac{h_w}{k} + 2d_c + 8g_w - l_{g,cmi} \right) \tag{18}$$

The losses are based on the total of the core and copper losses given by:

$$P_{cu} = I_{rms,dmi}^2 \left(\frac{r_{cu} J_{cond}}{I_{rms,dmi}} \right) MLT_{dmi} n_{dmi} + I_{rms,cmi}^2 \left(\frac{r_{cu} J_{cond}}{I_{rms,cmi}} \right) MLT_{cmi} n_{cmi} \tag{19}$$

where r_{cu} is the conductor resistivity and should be modified depending on the relevant frequency and type of wire [4]. The DM inductors contains the fundamental and all switching harmonics, while the CM contains the fundamental and the triplen harmonics (for three interleaved windings). The harmonics will depend on the PWM modulation and can be derived for different strategies as in [5].

Core losses can be estimated as:

$$P_{fe} = 0.5 k_1 B_{max,dmi}^{\beta} f_{sw}^{\alpha} M_{fe,dmi} + 0.5 k_1 \left(\frac{B_{max,cmi}}{3} \right)^{\beta} f_g^{\alpha} M_{fe,dmi} + 0.5 k_1 B_{max,cmi}^{\beta} f_g^{\alpha} M_{fe,cmi} \tag{20}$$

where k_1, α, and β are Steinmetz constants that depend on the material, f_{sw} is the switching frequency of the interleaved converter, and f_g is the frequency of the grid. The flux in the differential part contains the non-triplen harmonics plus additional fundamental and triplen harmonics coming from the CM coupling, but split equally in the different branches. The CM core section should contain mainly the fundamental and triplen harmonics.

It should be noted that in (20) the losses are calculated using the Steinmetz equation considering separately the losses from the low frequency and high frequency harmonics. The result will not be completely accurate when there is a high percentage of low frequency flux but it is sufficient for a preliminary estimate.

The final step of the optimization is to ensure the maximum temperature of the inductor is within the limits of the materials, such as that described in [6]. In the example for this paper then the weighting function for losses was adjusted to keep the temperature rise in the core or conductor equal to 40°C.

4 Design Comparison

Using the equations given in Sec. 3, designs were made for a grid converter application consisting of three interleaved sections, and with a total rated power of 120 kW and connected to a 400V, 50 Hz grid and considering sinusoidal PWM with a switching frequency of 48 kHz. The actual filter requirements will depend on the grid and it is possible to use a complete inductive design or a higher order filter consisting of multiple components. An example filter is given in Sec. 4.4 although the complete design of the filter is outside the scope of this work. Instead this section focuses on studying the overall effects of varying the CM and DM inductor sizes on the inductor size. The tools and procedures developed here could then be applied as part of a complete optimization of the converter filter for any specific grid requirements.

The designs are based around a reference design considering a required 50 µH CM inductance and 200 µH DM inductance. Secs. 4.1 and 4.2 consider inductors with nanocrystalline cores (kOr 120), while Sec. 4.3 considers other materials and methods to optimize core utilization.

4.1 Differential Mode Inductance Variation

Variation of the DM inductance will directly impact the peak circulating currents. These currents flow through the devices, and therefore any large increase in circulating current will increase both conduction and switching losses. Fig. 5 shows changes in inductor size for a DM inductance varying from 50 to 500 µH, as well as the peak circulating current. The CM inductance was fixed at 50 µH.

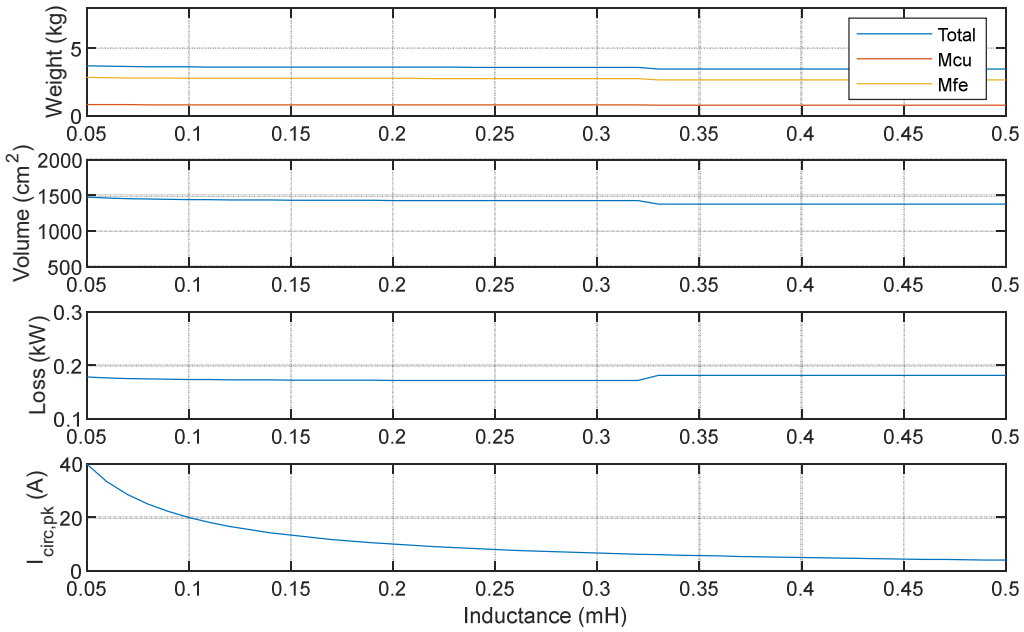

Fig. 5. Inductor size, weight and losses for varying differential mode inductance.

It can also be seen that the weight, volume and losses don't change much for different DM inductance. The inductance and peak current are inversely proportional so that from (**1**) and (**2**), increasing the inductance by reducing the air gap will result in a similar peak flux density. Eventually at high inductances then the air gap will reach a minimum value, the core reluctance will become more important, and then more turns will be required to further increase the inductance, resulting in increasing weight, volume, and/or losses.

Since converter losses generally increase with reduced inductance (due to higher ripple current) in the devices then there is an overall benefit to maximizing the DM inductance within construction limits.

4.2 Common Mode Inductance Variation

Variation of the CM inductance produces a more important change in the inductor size since there is no corresponding reduction of peak flux generating current such as in the differential design. Resulting weight, volume, and losses of the inductor are shown in Fig. 6 for a fixed DM inductance of 200 µH and CM inductance varying from 10 to 100 µH (equivalent to 0.2 – 1.5 % impedance range).

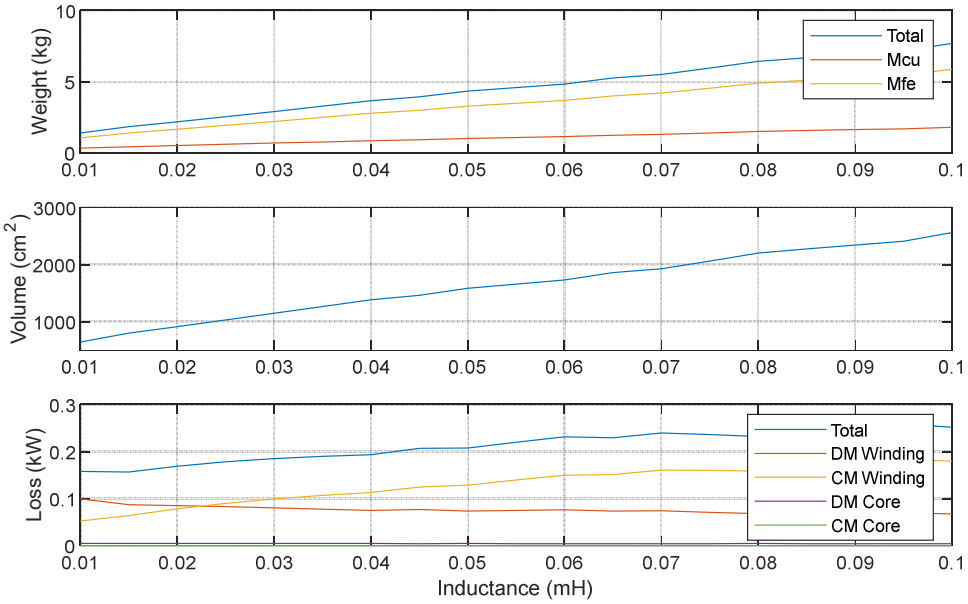

Fig. 6. Inductor size, weight and losses for varying common mode inductance.

Losses are dominated by winding losses, which must support the full current and all high frequency harmonics and the DM core, which has only high frequency flux. Losses slightly increase at low inductance since this low inductance leads to lower attenuation of triplen harmonics, which are only affected by the CM inductance. Core losses are very insignificant due to the fact that the nanocrystalline has excellent performance at high frequency and the actual percentage of high-frequency flux is fairly low, even in the DM part (the CM part has only a small amount of triplen harmonics).

This indicates a potentially important benefit from using a silicon steel core, which would allow higher flux densities and would have the effect of reducing overall inductor costs (estimated to be as high as 8x larger in [7]).

4.3 Core Optimization

A second key optimization possibility can be where it can be seen that the CM core will normally have only CM flux, which is mostly due to 50 Hz AC current. This low frequency flux would allow optimizing the inductor design by using a plated steel core in the CM branch, while using a higher frequency material only in the DM section.

Design results in Fig. 7 using a 0.2 mm plated Grain Oriented Electrical Steel show an improvement in weight, volume, and losses, except for low inductances where the higher switching harmonics results in increase core losses. Core losses in the CM core are still low, with only a small increase at low inductances due to the higher switching ripple frequencies.

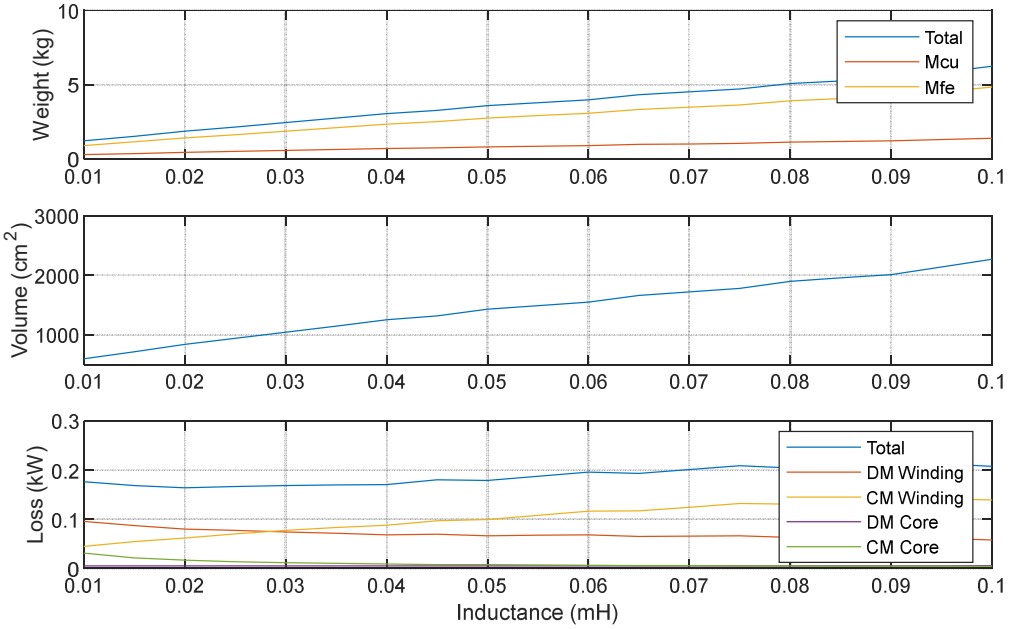

Fig. 7. Inductor size, weight and losses with a Si-Steel CM Core Section.

In fact further increases are possible if the entire core is made from Si-Steel (both DM and CM sections). The DM section of the core contains a large CM flux, so that the high frequency DM flux represents only a small percentage of the overall flux. It will result in higher losses but could offer a reduction in volume of >50%.

One final aspect of the interleaved converter is that the highest circulating current in the coupled inductors occurs at the zero crossing of the voltage. When the converter has mostly active power, then this implies that peak flux of the CM and DM parts occurs at different times, offering potential for overall core size optimization.

In the optimal case where k_r in (7) is equal to 2/3 then the resulting design shows a reduction similar to using the silicon steel CM core. The two techniques can both be applied resulting in an even smaller design, as shown in Fig. 8 compared with Fig. 6.

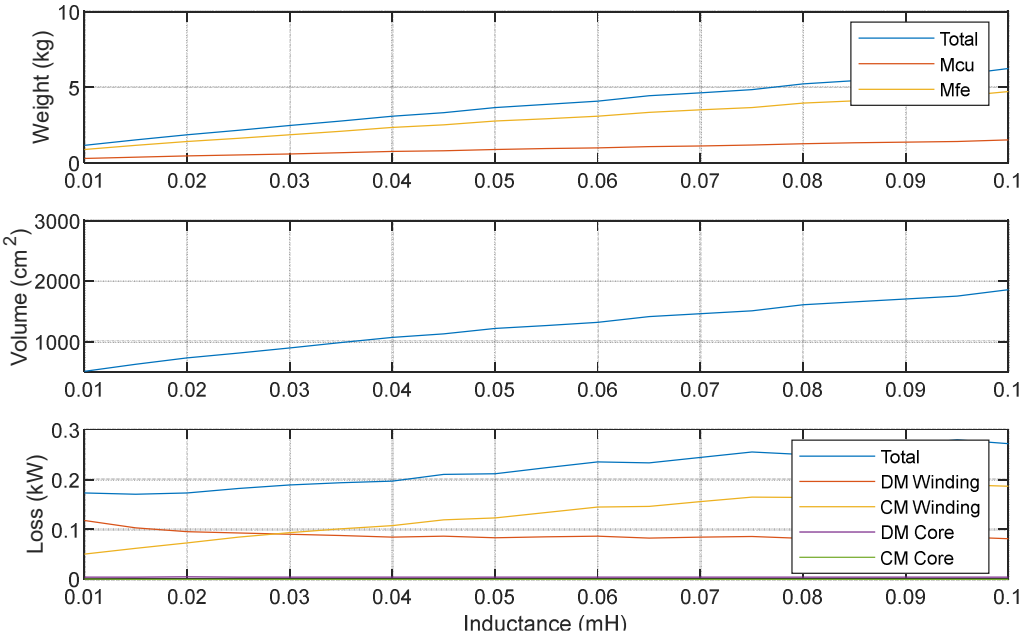

Fig. 8. Inductor size, weight and losses with a steel core and minimal reactive power.

4.4 Comparison with other Inductor Designs in a Grid Filter Application

In order to compare with other designs, then similar cost minimization functions were created to achieve 200 µH DM inductance and for varying CM inductance. Three cases are compared:

1. Case 1: 3-phase Inductor + 3x coupled inductor + CM Choke
2. Case 2: 3x coupled inductor with CM core (Fig. 2a) + CM Choke
3. Case 3: 3x coupled inductor with wound CM core (Fig. 2b) + CM Choke

A general illustration of the combined filter concepts is shown in Fig. 7.

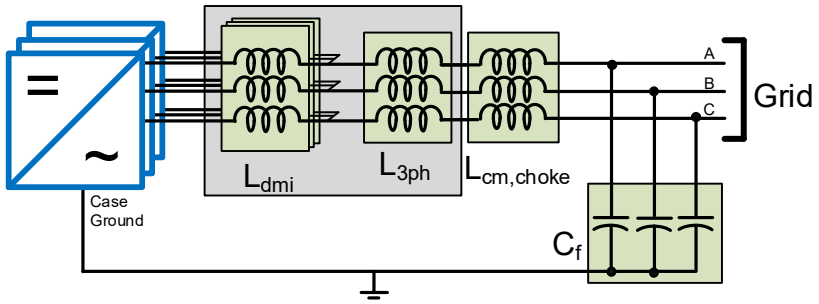

Fig. 9. Example filter concept circuit diagram.

The CM choke is for filtering 3rd harmonic (and other triplen harmonics) which are not attenuated by the DM or 3-phase inductors. For Case 1 it is set to 250 µH, for Cases 2 and 3, the total of the CM choke and CM inductance of the combined inductor kept constant at 250 µH. The CM filter capacitor (C_f) is not sized since it will be the same in all cases. As noted previously, the actual size requirements of the different components depend on the filter requirements to meet the grid code. Since all three cases are designed to the same requirement then it represents a valid comparison of the different filters, although the difference in benefits will vary for different applications.

Comparison of the volume is more difficult due to integration of separate components in Case 1 and therefore only the total weight of the core and conductor and full-load losses are shown. The optimizer was weighted toward minimum weight and in all cases the maximum temperature rise in the core or winding was kept to 40ºC. Results are shown in Fig. 10, note that total weight and losses is of all core and windings for all inductor sections.

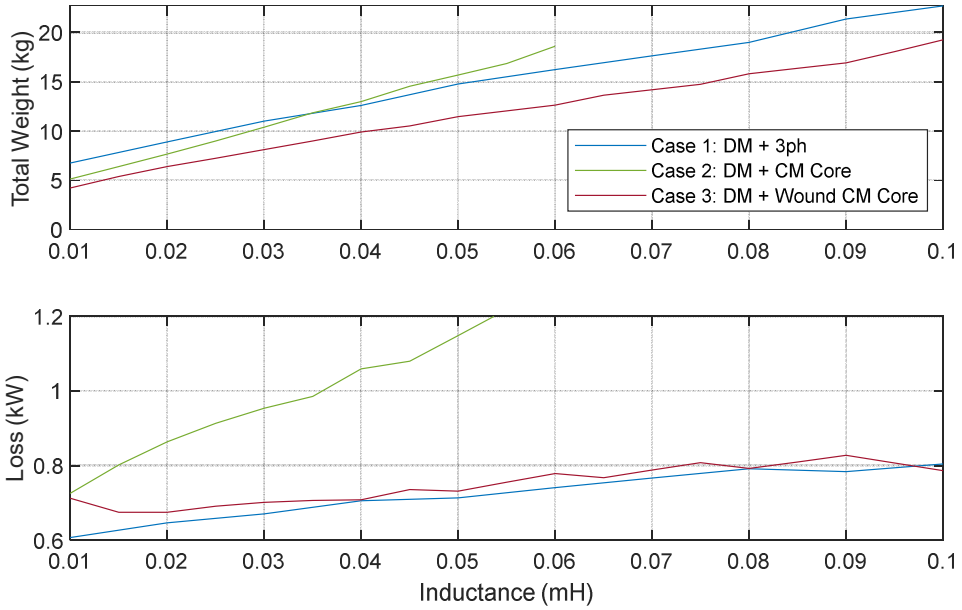

Fig. 10. Comparison of total inductor weight and losses.

The results show that the combined CM and DM (Case 3) design can potentially offer lower losses and weight compared to a conventional 3-phase design with separate coupled inductors. The unwound core design (Case 2: CMDM) achieves similar results to Case 3 at low inductance, but achieving higher CM inductance with only the additional core section results in higher losses in the DM winding (due to increased turns). It can also be seen that using separate inductors is still competitive, although overall weight is higher. An advantage of the separate inductors will be lower overall cost due to use of standard core sections.

It should also be noted that the CM inductance provides the main inductance at the grid frequency (50 Hz in our case) while providing very little benefit as a filter (non-triplen harmonics are cancelled after the DM inductor and triplen harmonics are not affected by the 3-phase inductor, only the CM choke). The resulting size is then mainly determined by the speed of the control or peak current during faults (which is also impacted by the control speed). A smaller inductance will offer a faster response, but also requires higher performance from the converter controller and sensors.

5 Experimental Results

A 3-phase interleaved converter was tested in the lab to verify the operation. The design uses a 200 uH coupled inductor with an additional 65 µH external inductor (type N CNW 854 / 250, not shown), corresponding to Case 1.

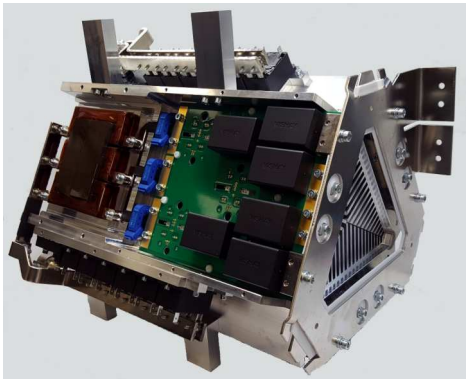

(a) Converter hardware

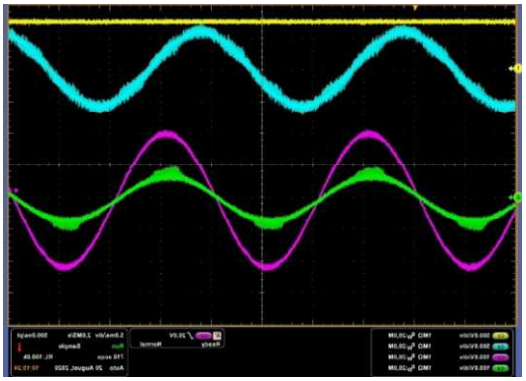

(b) Test results (Yellow: DC Link Voltage, Blue: AC voltage, Purple: AC grid current, Green: Coupled Inductor current

Fig. 11. Converter and test results.

It can be seen in Fig. 11a that the converter, DC link capacitors, and interleaved inductor were built into a common hardware design, resulting in a compact converter with a simple cooling system for both power devices and coupled inductor.

The resulting operation is shown in Fig. 11b where it can be seen that the highest ripple current in the coupled inductor occurs at the peak AC current. This is due to reactive power operation (the highest DM current is at the zero crossing of the voltage) and represents the case where no additional optimization of the core can be performed (such as STATCOM applications).

6 Conclusions

The analysis shows overall benefit for an inductor design combining the DM inductance with a wound CM limb. Splitting the inductors is still competitive and may have an overall lower cost, which may be the key criteria for some applications.

Comparing the combined inductors, losses in the unwound core design (Case 2) greatly increase for high CM inductances. When the core is wound (Case 3) then the extra degree of freedom allows the overall best design. Further improvements can be obtained by (a) using a high flux density core for the CM limb, (b) using a high flux density core for the whole inductor (trading off size with losses), (c) taking advantage of the phase shift in peak flux density between the DM and CM sections in applications with mostly real power.

While the results are interesting, test results are shown just with the split inductor case and work is ongoing on innovative methods to construct the combined inductor with the converter.

7 References

[1] G. Mondal, J. Robinson, S. Haensel, M. Neumeister, and S. Nielebock, 'On Optimal Construction of Interleaved Converter for minimum Circulating Current', in *2018 20th European Conference on Power Electronics and Applications (EPE'18 ECCE Europe)*, Sep. 2018, p. P.1-P.10.

[2] G. Mondal, J. Robinson, and S. Haensel, 'Design and Verification of Compact Inductor for Interleaved AC/DC Converter', in *2019 21st European Conference on Power Electronics and Applications (EPE '19 ECCE Europe)*, Sep. 2019, p. P.1-P.9. doi: 10.23919/EPE.2019.8915512.

[3] K.-B. Park, F. D. Kieferndorf, U. Drofenik, S. Pettersson, and F. Canales, 'Optimization of LCL Filter With Integrated Intercell Transformer for Two-Interleaved High-Power Grid-Tied Converters', *IEEE Trans. Power Electron.*, vol. 35, no. 3, pp. 2317–2333, Mar. 2020, doi: 10.1109/TPEL.2019.2926312.

[4] M. Bartoli, N. Noferi, A. Reatti, and M. K. Kazimierczuk, 'Modeling Litz-wire winding losses in high-frequency power inductors', in *PESC Record. 27th Annual IEEE Power Electronics Specialists Conference*, Jun. 1996, vol. 2, pp. 1690–1696 vol.2. doi: 10.1109/PESC.1996.548808.

[5] G. Holmes and T. Lipo, *Pulse Width Modulation for Power Converters: Principles and Practice*. 2003.

[6] M. Sippola and R. E. Sepponen, 'Accurate prediction of high-frequency power-transformer losses and temperature rise', *IEEE Trans. Power Electron.*, vol. 17, no. 5, pp. 835–847, Sep. 2002, doi: 10.1109/TPEL.2002.802193.

[7] D. Ruiz-Robles, J. Ortíz-Marín, V. Venegas-Rebollar, E. L. Moreno-Goytia, D. Granados-Lieberman, and J. R. Rodríguez-Rodriguez, 'Nanocrystalline and Silicon Steel Medium-Frequency Transformers Applied to DC-DC Converters: Analysis and Experimental Comparison', *Energies*, vol. 12, no. 11, 2019, doi: 10.3390/en12112062.